White Light Interferometry of SOI Deeply-Etched Fully Integrated MEMS Interferometers

Haitham Omran,

Laboratory of Micro Optic, Faculty of Information Engineering and Technology, German University in Cairo, Egypt

haitham.omran@guc.edu.eg

and

Diaa Khalil,

Faculty of Engineering, Ain Shams University, Egypt

diaa.khalil@ieee.org

Abstract: In this paper we investigate numerically and experimentally the effect of thin Silicon (Si) splitter parasitic Fabry-Perot and Si/Air splitter Silicon dispersion on the white light interferometry of deeply-etched MEMS interferometers using Silicon On Insulator (SOI) technology. The numerical simulations and practical measurements show that multiple internal reflections inside the thin Silicon splitter form a parasitic Fabry-Perot cavity inside the MEMS interferometer. This results in duplicated side interferograms that practically limits the interferometer maximum optical path difference and hence the resolution of MEMS based FT-IR spectrometer. Silicon dispersion, in case of Si/Air splitter results in a chirped and shifted interferogram that can be compensated using very long travel range electrostatic MEMS actuators.

Keywords: White Light, Dispersion, Interferometer, MEMS, SOI, Deeply-Etched.

قياس تداخل الضوء الأبيض في مقياس تداخل ضوئي كهروميكانيكي ميكرومتري مصنع بتكنولوجيا الحفر العميق على السيليكون

الملخص: يقوم هذا البحث بعرض محاكاة رقمية وتجارب عملية تبين تأثير التشتت الضوئي على عمل مقسم ضوئي مصنوع بتكنولوجيا الحفر العميق على السيليكون وتأثير التشتت على عمل مقياس تداخل ضوئي كهروميكانيكي ميكرومتري. وتخلص الدراسة إلى أن التشتت الضوئي الناتج عن استخدام السطح البيني بين الهواء والسيليكون كمقسم ضوئي يمكن التغلب عليه باستخدام محرك كهروميكانيكي ميكرومتري بسعة حركة خطية كبيرة. أما التشتت الضوئى الناتج عن مقسم رفيع من السيليكون فيؤدي إلى ظهور تداخل جانبي غير مرغوم فيه مما يؤثر على دقة مقياس التداخل الضوئي.

1. Introduction

Deeply-Etched optical MEMS interferometers and filters using Deep Reactive Ion Etching [1- 5] (DRIE) of SOI [6, 7] wafers have become one of the most enabling technologies for FT-IR micro-spectrometers [8-15] and MEMS based Swept Lasers [16- 18]. Fully integrated deeply-etched Michelson [8] and Mach-Zhender [11] MEMS interferometers have been implemented using this technology and used for MEMS based FT-IR spectroscopy. Two types of deeply-etched splitters have been presented in literature: thin Si splitter [10] and Si/Air beam splitter [8]. A scientific study comparing the performance of deeply-etched interferometers using these two types of splitters with a white light input [23-29] has not been presented in literature, far to our knowledge. The operation of MEMS interferometers with the two splitter types have only been studied using a monochromatic input source [8-13]. The target of this paper is to compare the performance of deeply-etched MEMS interferometers with thin Silicon and Si/air beam splitters with a white light input. The comparison focuses on two main effects: The first is the effect of parasitic Fabry-Perot (FP) cavity formed by the thin Si splitter and the second is the effect of Silicon dispersion in Si/air beam splitter, both on the MEMS interferometer output interferogram.

The comparison is done with the Si/air splitter in a Mach-Zhender Interferometer (MZI) configuration while the thin splitter in a Michelson Interferometer (MSI). The fabrication of MZI with two thin splitters would double the problem of parasitic FP. The two splitters will not have exact dimensions due to DRIE errors imposing additional unknowns to the study in addition to introducing robustness issues. These reasons motivated the use of two different configurations for the study.

The first section of the paper describes the two MEMS interferometers with the two splitter types. The second section explains the parasitic FP and dispersion effects caused by the two splitters and provides the mathematical representation of the output interferogram. The third section estimates the two effects using numerical simulations and the last section presents the practical measurements of the output interferogram of the two interferometers with white light input and compares the results with the numerical simulations. Part of the numerical results about dispersion in Mach-Zhender interferometry has been presented in MOC2017 Conference in Japan [30]. The numerical analysis of thin Si splitter effect, detailed analysis of Si/Air splitter dispersion effect and all practical results are all new additions.

2. Deeply etched interferometers

The two deeply etched interferometers under consideration are a MSI with thin Silicon beam splitter and a MZI with two Si/Air beam splitters. The layouts of the two deeply etched interferometers are shown in figure 1 and figure 2. The fabrication steps have been discussed in our previous work [8, 11]. The Michelson interferometer consists of a moving mirror M1, a fixed mirror M2, thin Silicon splitter BS and two input and output fiber grooves. The optical path (L1,L2) of the two beams is designed to be equal. However after fabrication a mismatch may occur due to DRIE over etching errors. Also misalignment of the input fiber core form mean ray position at the center of the splitter may cause additional optical path mismatch.

The MZI consists of two Si/Air beam splitters BS1 and BS2, two moving mirrors M1 and M2, a total internal reflection (TIR) mirror M3, an input fiber groove and two output fiber grooves [11]. The two mirrors can be moved at the same time using the same MEMS electrostatic comb actuator. Recording the output power with the motion of the moving mirrors gives the interferogram of an FT-IR spectrometer [11].

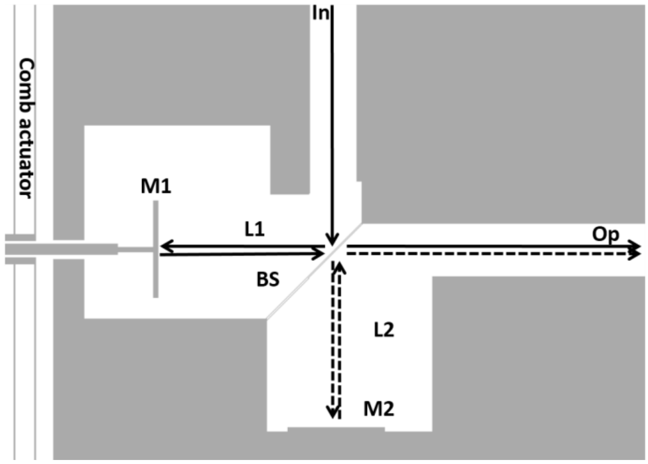

Figure 1. Layout of Deeply-etched Michelson interferometer with thin Silicon beam splitter.

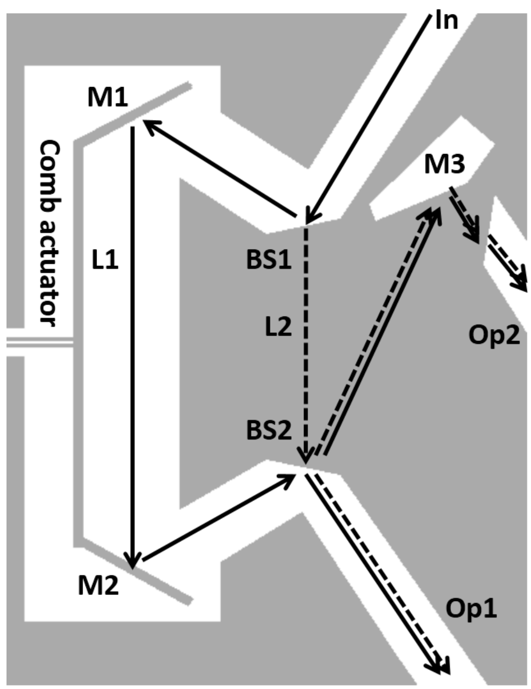

Figure 2. Layout of deeply- etched Mach-Zhender interferometer with two Si/Air beam splitters.

3. Description of parasitic Fabry-Perot and Dispersion Effect

3.1 Parasitic FP effect in thin Si splitter

The thin silicon splitter has two Si/air interfaces parallel to each other and aligned by optical lithography with a thin layer of Silicon separating them. The multiple reflections in this thin Silicon layer forms the parasitic Fabry-Perot effect. In conventional bulk spectrometers this can be easily overcome by Antireflection (AR) coating one side of the splitter to match air. This is not feasible in a deeply etched MEMS interferometer fabricated in a one lithography step using DRIE. A subsequent coating step will also coat the micro mirrors in front of the splitter from both sides in addition to introducing uniformity issues in an in-plane deep structure. The complex amplitude of the electric field at output of the Michelson interferometer with thin Si splitter assuming a plane wave model is given by:

$$E_{op} = E_{in} r_{fp} t_{fp} \exp\left[-j\frac{2\pi}{\lambda}\left(L_{in} + 2L_1 + L_{op} + MOPD \right) - j\pi \right]$$
$$+ E_{in} r_{fp} t_{fp} \exp\left[-j\frac{2\pi}{\lambda}\left(L_{in} + 2L_2 + L_{op} + OPM \right) - j\pi \right]$$

where t_{fp} and r_{fp} are wavelength dependent transmission and reflection coefficients for a Fabry-Perot cavity with an arbitrary incident angle θ [21]. t_{fp} and r_{fp} are given by:

$$t_{fp} = \frac{t_{12} t_{21} r_{21}}{1 - r^2_{21} \exp(j\, 2\eta d\, \frac{2\pi}{\lambda} \cos\theta)} \exp(j\eta \frac{2\pi}{\lambda} \frac{d}{\cos\theta})$$

$$r_{fp} = r_{12} + \frac{t_{12} t_{21}}{1 - r^2_{21} \exp(j\, 2\eta d\, \frac{2\pi}{\lambda} \cos\theta)} \exp(j\, 2\eta d\, \frac{2\pi}{\lambda} \cos\theta)$$

L1 and L2 are the length between thin splitter and first and second mirrors respectively as indicated in figure 1. MOPD is the optical path difference due to mirror retardation which is double the comb displacement. Lin and Lop are the length of input and output grooves till fiber tip respectively. OPM is the optical path mismatch between L1 and L2 caused by DRIE errors, fibers misalignment and verticality of deeply-etched surfaces. The π factor accounts for a π phase shift at the mirror [21]. (r_{12},t_{12}) and (r_{21},t_{21}) are the Fresnel reflection and transmission coefficient from air to Silicon and from Silicon to air respectively [20]. d is thickness of the thin Silicon splitter.

3.2 Dispersion Effect in Si/Air Splitter

The dispersion effect in case of the MZI with two Si/Air beam splitter rises from the fact that one of the optical beams has its optical path completely in Silicon with wavelength dependent refractive index while the other beam is completely in air. The monolithic integration of the MZI with thick splitter using DRIE causes this effect to be inherited in the structure. Si cannot be placed in the air path as it will cause multiple parasitic coupled cavities with the moving micro mirrors and loss of power in path L1. At the first output of the MZ interferometer with Si/Air beam splitter the electric field is given by:

$$E_{op1} = E_{in} r_{s1} r_{s2} \exp\left[-j\frac{2\pi}{\lambda}\left(L_{in} + L_1 + L_{op} + MOPD + L_{op1}\right) + j\pi\right]$$
$$+ E_{in} t_{s1} t_{s2} \exp\left[-j\frac{2\pi}{\lambda}\left(L_{in} + \eta(\lambda) L_2 + L_{op} + L_{op1}\right)\right]$$

where (t_{s1},r_{s1}), (t_{s2},r_{s2}) are the transmission and reflection coefficient at the first Air/Si (BS1) and second Si/Air (BS2) beam splitters, respectively calculated from Fresnel equations [20]. A π /2 phase exists between the reflected and transmitted beams at each beam splitter [21]. The intensity of the interferogram at the output is given by:

$$I_{op1} = | E_{op1} |^2$$

The wavelength dependent refractive index can be calculated from a temperature dependent Sellmeier model [22]:

$$\eta^2(\lambda, T) = 1 + \sum_{i=1}^{3} \frac{S_i(T).\lambda^2}{\lambda^2 - \lambda^2_i(T)}$$

where Si are the strengths of the resonance features in the material at wavelengths λi and T is the temperature which is assumed to be 300 K.

4. Numerical model

4.1 Numerical estimation of parasitic FP effect

To numerically investigate the parasitic FP and dispersion effects a simple plane wave model was used based on the equations in the previous section. The new additions in the model are the wavelength dependent refractive index $\eta(\lambda)$ and the embedded parasitic FP effect in rfp and tfp. A white light input is assumed in the wavelength range 1.2 um to 1.7 um with equal amplitude for all wavelengths. The numerical simulator computes the electric field for each input wavelength at the output of the interferometers. All field components are then added and intensity is calculated. L1 and L2 of the MSI are designed to be 650 um. The thin splitter thickness after fabrication is estimated to be 2.5 um. Measured MOPD of the comb actuator is 50 um. OPM is estimated to be 26 um to fit with experimental results. This value is reasonable as the error in DRIE process is proportional to the size of the area to be etched [11], fibers misalignment and verticality of the deeply-etched surfaces. The simulated interferogram at the output of the MSI is shown in figure 3. It is clear that the parasitic FP causes duplicated side interferograms to appear limiting the useful optical path difference of the interferometer and hence resolution in case of FT-IR spectroscopy [21]. The location of the duplicated interferograms is function of the splitter thickness.

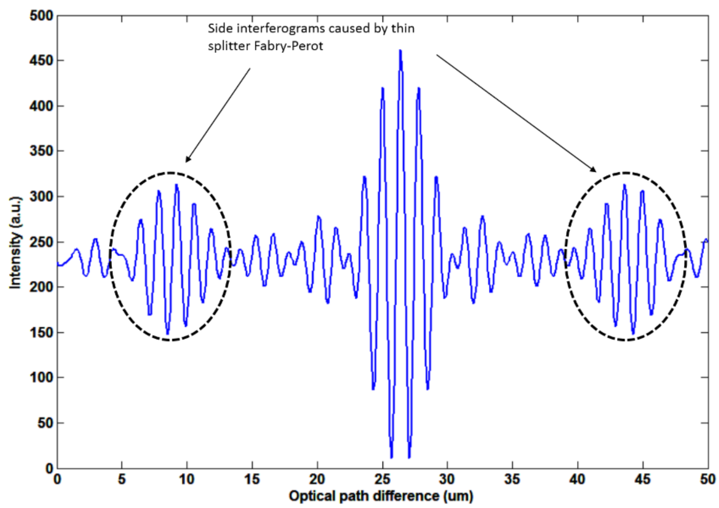

Figure 3.Numerically simulated interferogram of deeply-etched MSI showing duplicated side interferograms.

4.2 Numerical Estimation of Dispersion Effect

For the MZI, the comb actuator OPD is 130 um [11]. The interferogram at the first output was simulated for the 130 um OPD that can be practical achieved by the comb and a theoretical extension of 350 um as shown in Figure 4. The Si dispersion effect causes the interfergram to be chirped and shifted. For an OPD of 130 um, part of the intereferogram is practically outside the achievable 130 um OPD. Thus the dispersion effect of the Si/Air beam splitter needs to be compensated by long travel range electrostatic comb actuators with about 250 um OPD.

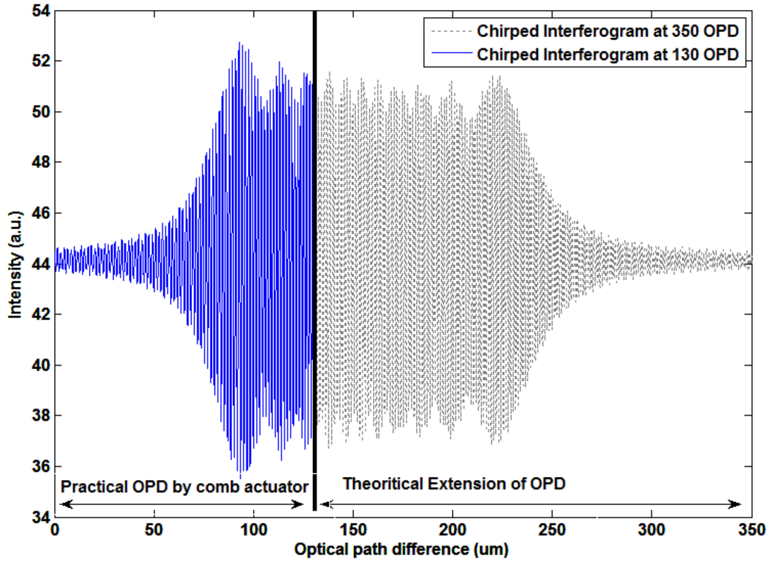

Figure 4. Numerically simulated interferogram of deeply-etched MZI showing chirped and shifted interferogram.

5. Practical measurements of white light interferogram

The setup used in the characterization is shown in figure 5. It consist of a white input source with tungsten lamp (1.2 um – 1.7 um), multimode fibers with 62.5 um core inserted into the micromachined grooves aligned with the interferometer splitter, an Agilent optical InGaAs detector connected to a GPIB interface with personal computer and 5 degree-of-freedom micro positioners for fiber alignment.

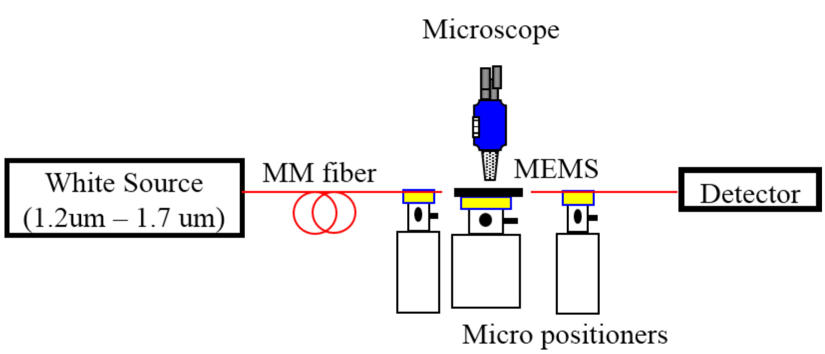

Figure 5. Characterization Setup

Measured interferogram of the MSI is shown in figure 6. The interferogram appears with side duplicated interferograms caused by parasitic FP effect as expected. Their location depends on real thickness of the thin Si splitter after fabrication. The ZOPD position is shifted by 26 um due to fiber misalignment and etching error as discussed before. The difference between the measured side interferograms and numerical simulation is attributed to the beam divergence in the micro optical structure with increasing OPD which has not been accounted for in the numerical model. The glitches may be caused by mirror vibration at the start of actuation or contamination particles in the structure after words as the interferometer is not caped and tested in a non clean room. For the MZ interferometer the measured interferogram after numerically removing the effect of decay in the measured power with increasing OPD is shown in figure 7.

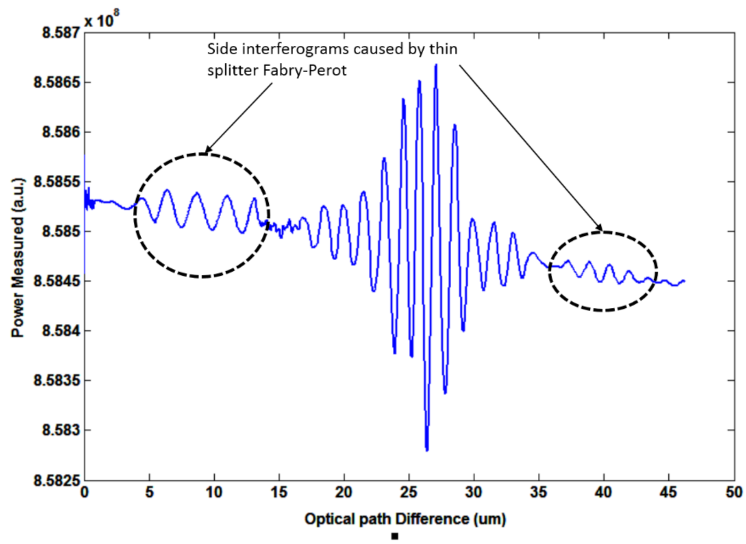

Figure 6. Measured interferogram of MEMS MSI with thin Silicon splitter showing the effect of parasitic FP.

The white light input source power is about -60 dBm and the MZ interferometer loss is around 10 dB [6] causing the amplitude of the output interferogram to be very low and measured power to be comparable to the noise level. The final step is to calculate the absolute of complex Fast Fourier Transform (FFT) to compensate for dispersion effect, and remove undesired noise as shown in figure 8.

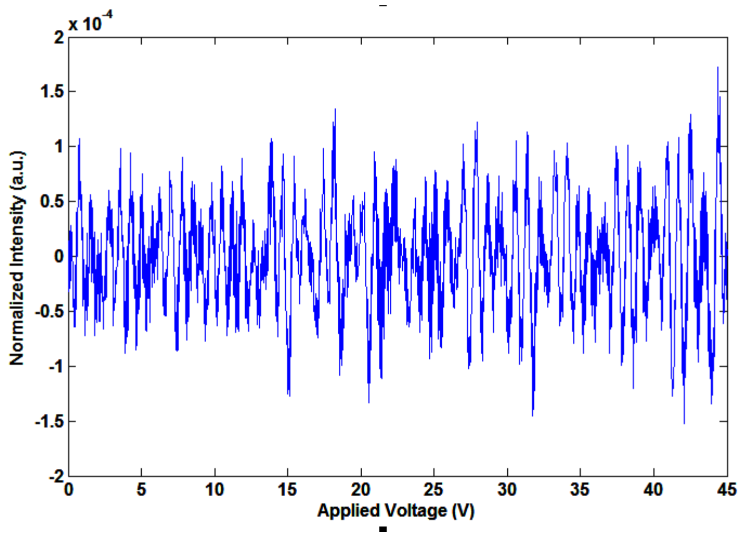

Figure 7. Measured interferogram of MEMS MZI with Si/air splitters showing dispersion effect.

The MZI output Power Spectral Density (PSD) agrees with the MSI PSD for long wavelength while in the short wavelengths some defects appear for the MZI as shown in figure 8. We attribute this to the limited OPD (130 um) of the MZI causing the chirped interferogram to be only partially collected.

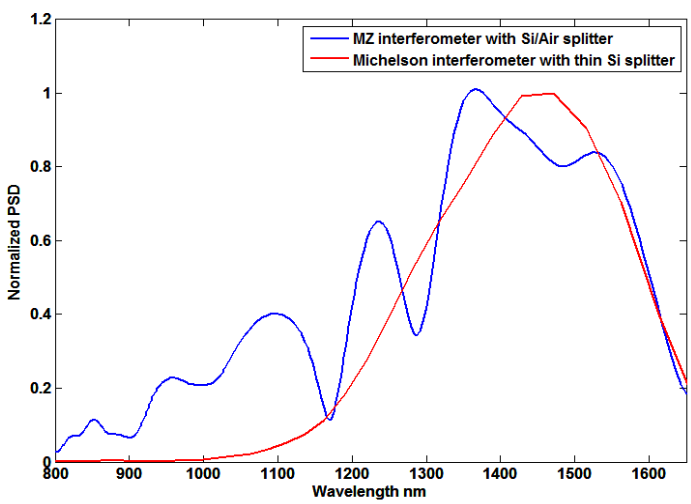

Figure 8. Interferogram FFT for thin Silicon and Si/Air beam splitter interferometers.

6. Conclusion

We have presented numerical and practical study on white light interferometry of SOI deeply-etched fully integrated MEMS interferometers. The thin Silicon splitter causes a parasitic Fabry-Perot effect that results in duplicated side interferoargam which limits the useful OPD and hence resolution of an FT-IR spectrometer. The Si/Air splitter suffers from dispersion effect that can be compensated using long travel range actuators making it the better choice for an FT-IR spectrometer in terms of optical resolution, robustness and reliability.

7. References

[1] A. Fathy, Y. M. Sabry, M. Amr, M. Gnambodoe-Capo-chichi, M. Anwar, A. O. Ghoname, A. Amr, A. Saeed, M. Gad, M. Al Haron, M. Erfan, Y. Leprince-Wang, B. Saadany, D.Khalil, and T. Bourouina "MEMS FTIR optical spectrometer enables detection of volatile organic compounds (VOCs) in part-per-billion (ppb) range for air quality monitoring", Proc. SPIE 10931, MOEMS and Miniaturized Systems XVIII, 1093109 (4 March 2019); doi: 10.1117/12.2508239; https://doi.org/10.1117/12.2508239

[2] F. Marty, L. Rousseau, B. Saadany, B. Mercier, O. Français, Y. Mita and T. Bourouina, "Advanced etching of silicon based on deep reactive ion etching for silicon high aspect ratio microstructures and three-dimensional micro-and nanostructures." Microelectronics journal 36.7 (2005): 673-677.

[3] B. Saadany, D. Khalil and T. Bourouina,"Highly efficient micromachined bragg mirrors using advanced DRIE process." MEMS, NANO and Smart Systems, The 2006 International Conference on. IEEE, 2006.

[4] Amr O. Ghoname, Yasser M. Sabry, Momen Anwar, Ahmed Saeed, Bassam Saadany, and Diaa Khalil "Ultra wide band MIR MEMS FTIR spectrometer", Proc. SPIE 10931, MOEMS and Miniaturized Systems XVIII, 109310Z (4 March 2019); doi: 10.1117/12.2509378; https://doi.org/10.1117/12.2509378

[5] Ahmad Mahfouz, Haitham Omran, Yasser M. Sabry, Diaa Khalil, Frédéric Marty, and Tarik Bourouina "Deeply etched silicon optical cavity with curved slotted micromirrors (Conference Presentation)", Proc. SPIE 10931, MOEMS and Miniaturized Systems XVIII, 109310N (4 March 2019); doi: 10.1117/12.2508208; https://doi.org/10.1117/12.2508208

[6] W. Noell, W. Sun, N. de Rooij, H. P. Herzig, O. Manzardo, and R. Dandliker, "Optical mems based on silicon-on-insulator (SOI) for monolithic microoptics." Lasers and Electro-Optics Society (LEOS). The 15th Annual Meeting of the IEEE. Vol. 2. Institute of Electrical and Electronics Engineers (IEEE), 2002.

[7] W. Noell, P.-A. Clerc, L. Dellmann, B. Guldimann, H.-P. Herzig, O. Manzardo, C. R. Marxer, K. J. Weible, R. Dandliker, and N. de Rooij "Applications of SOI-based optical MEMS." IEEE Journal of selected topics in quantum electronics 8.1 (2002): 148-154.

[8] B. Saadany, H. Omran, M. Medhat, F. Marty, D. Khalil, and T.Bourouina,"MEMS tunable Michelson interferometer with robust beam splitting architecture." Optical MEMS and Nanophotonics, 2009 IEEE/LEOS International Conference on. IEEE, 2009.

[9] B. Mortada, M. Erfan, M. Medhat, Y. M. Sabry, B. Saadany and D. Khalil, "Wideband optical MEMS interferometer enabled by multimode interference waveguides." Journal of Lightwave Technology 34.9 (2016): 2145-2151.

[10] Yu, Kyoungsik, Daesung Lee, Uma Krishnamoorthy, Namkyoo Park, and Olav Solgaard, "Micromachined Fourier transform spectrometer on silicon optical bench platform." Sensors and Actuators A: Physical 130 (2006): 523-530.

[11] H. Omran, M. Medhat, B. Mortada, B. Saadany, and D. Khalil, "Fully integrated Mach-Zhender MEMS interferometer with two complementary outputs." IEEE Journal of Quantum Electronics 48.2 (2012): 244-251.

[12] D. Khalil, H. Omran, M. Medhat, B. Saadany, "Miniaturized tunable integrated Mach-Zehnder MEMS interferometer for spectrometer applications." MOEMS and Miniaturized Systems IX. Vol. 7594. International Society for Optics and Photonics, 2010.

[13] H. Omran, M. Medhat, B. Saadany, D. Khalil, "Mach-Zehnder MEMS interferometer with two Si/Air beam splitters." Design and Test Workshop (IDT), 2009 4th International. IEEE, 2009.

[14] Yasser M. Sabry, D. Khalil and T. Bourouina, "Monolithic silicon-micromachined free-space optical interferometers onchip." Laser & Photonics Reviews 9.1 (2015): 1-24.

[15] M. Erfan, Yasser M Sabry, M. Sakr, B. Mortada, M. Medhat and D. Khalil, "On-chip micro–electro–mechanical system fourier transform infrared (MEMS FT-IR) spectrometer-based gas sensing." Applied spectroscopy 70.5 (2016): 897-904.

[16] H. Omran, Y. M. Sabry, M. Sadek, K. Hassan and D. Khalil, "Wideband subwavelength deeply etched multilayer silicon mirrors for tunable optical filters and SS-OCT applications." IEEE Journal of Selected Topics in Quantum Electronics 21.4 (2015): 157-164.

[17] H. Omran, Y. M. Sabry, M. Sadek, K. Hassan, M. Y. Shalaby and D. Khalil, "Deeply-etched optical MEMS tunable filter for swept laser source applications." IEEE Photonics Technology Letters 26.1 (2014): 37-39.

[18] J. Masson, R. St-Gelais, A. Poulin, and Y. A. Peter, "Tunable fiber laser using a MEMS-based in plane Fabry-Pérot filter." IEEE Journal of Quantum Electronics 46.9 (2010): 1313-1319.

[19] R. St-Gelais, A. Poulin and Y. A. Peter, "Advances in modeling, design, and fabrication of

deep-etched multilayer resonators." Journal of Lightwave technology 30.12 (2012): 1900-1908.

[20] K. Iizuka, Elements of Photonics in Free Space and Special Media (John Wiley & Sons, New York, 2002) p. 166.

[21] P. R. Griffiths and De Haseth, Fourier Transform Infrared Spectrometry (John Wiley & Sons, New York, 2007) Vol. 171.

[22] J. Frey Bradley, B. Leviton Douglas, J. Madison Timothy, "Temperature-dependent absolute refractive index measurements of synthetic fused silica." Optomechanical Technologies for Astronomy. Vol. 6273. International Society for Optics and Photonics, 2006.

[23] L. M. Smith and Chris C. Dobson, "Absolute displacement measurements using modulation of the spectrum of white light in a Michelson interferometer." Applied Optics 28.16 (1989): 3339-3342.

[24] KG. Larkin, "Efficient nonlinear algorithm for envelope detection in white light interferometry." JOSA A 13.4 (1996): 832-843.

[25] U. Schnell, R. Dändliker, and S. Gray, "Dispersive white-light interferometry for absolute distance measurement with dielectric multilayer systems on the target." Optics Letters 21.7 (1996): 528-530.

[26] Mark Johnson, "White light interferometry." Fibre Optics' 90. Vol. 1314. International Society for Optics and Photonics, 1990.

[27] Scott Diddams and Jean-Claude Diels, "Dispersion measurements with white-light interferometry." JOSA B 13.6 (1996): 1120-1129.

[28] A. P. Kovács, K. Osvay, Zs. Bor, and R. Szipöcs, "Group-delay measurement on laser mirrors by spectrally resolved white-light interferometry." Optics letters 20.7 (1995): 788-790.

[29] Kentaro Totsu, Yoichi Haga and Masayoshi Esashi, "Ultra-miniature fiber-optic pressure sensor using white light interferometry." Journal of Micromechanics and Microengineering 15.1 (2004): 71.

[30] H. Omran, B. Mortada and D. Khalil, "Numerical estimation of dispersion effect in deeply-etched fully integrated MEMS Mach-Zhender interferometer," 2017 22nd Microoptics Conference (MOC), Tokyo, 2017, pp. 278-279.